

Cite this: *J. Mater. Chem. C*, 2019,  
7, 12290Received 23rd July 2019,  
Accepted 17th September 2019

DOI: 10.1039/c9tc04014e

rsc.li/materials-c

## A distorted lactam unit with intramolecular hydrogen bonds as the electron donor of polymer solar cells†

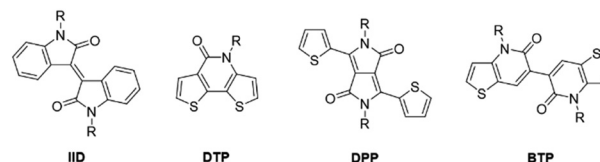
Hua-Chun Wang,<sup>a</sup> Minrun Ren,<sup>b</sup> Jian Cao,<sup>a</sup> Hong-Bo Yin,<sup>a</sup> Guichuan Zhang,<sup>b</sup>  
Jingyang Xiao,<sup>b</sup> Xiancheng Ren,<sup>a</sup> Hin-Lap Yip <sup>b</sup> and Yun-Xiang Xu <sup>\*a</sup>

A novel distorted lactam motif, namely 4,4'-dialkyl-[6,6'-bithieno[3,2-*b*]pyridine]-5,5'-(4*H*,4'*H*)-dione (BTP), could lock itself by intramolecular hydrogen bonds. In view of the potential of the motif, two D–A conjugated polymers, PBTD-BTP-HD and PBTD-BTP-OD, with two different long side chains consisting of 4,8-bis(5-(2-ethylhexyl)thiophen-2-yl)benzo[1,2-*b*:4,5-*b'*]dithiophene (BDT) as a donor unit and BTP as an acceptor unit were designed and synthesized. Furthermore, the photophysical, electrochemical and photovoltaic properties of both polymers were investigated. The morphologies and molecular ordering of the neat polymers and blend films were also probed to relate the side chain structures with aggregation states and device parameters. The device based on PBTD-BTP-OD with IT-M exhibited a power conversion efficiency of up to 9.54% thanks to the synergistic effect of the building blocks and side-chain engineering. As a result, it is successfully demonstrated that the novel distorted lactam BTP is a promising building block in organic solar cells.

## Introduction

Bulk heterojunction polymer solar cells (PSCs) consisting of electron donors and electron acceptors have drawn considerable interest due to their unique features, including flexibility, large-area fabrication, low cost and light weight.<sup>1–12</sup> At present, the power conversion efficiencies (PCEs) based on non-fullerene single-junction PSCs have exceeded 15%, which is benefited from the optimization of the device structure and the development of active layer materials, especially non-fullerene small molecular acceptor materials.<sup>13–17</sup> To match well with non-fullerene acceptors with strong absorption from 600 to 800 nm, it is very essential to design highly efficient wide bandgap polymer donors with suitable energy levels.<sup>7,18–20</sup>

Among the high-performance polymer donors, lactam skeletons, such as isoindigo (IID), dithieno[3,2-*b*:2',3'*d*]pyridin-5(4*H*)-one (DTP) and diketopyrrolopyrrole (DPP) (Scheme 1), have been considered as some of the most versatile and promising building blocks due to their strong electron-withdrawing properties and excellent planar



Scheme 1 Chemical structure of IID, DTP, DPP and BTP.

backbone.<sup>21–28</sup> Nevertheless, the highly planar building blocks often lead to excessive aggregation when the film is formed, which is not conducive to obtaining an optimized phase morphology for PSCs.<sup>29,30</sup> On the other side, an extensively distorted skeleton also leads to poor device performance due to insufficient intramolecular charge transport properties.<sup>31–33</sup> As a balance, a rigid distorted skeleton with a certain dihedral angle may be a desirable motif to achieve appropriate polymer chain conformation and aggregation states.<sup>34,35</sup> Traditionally, DPP lactam units are propitious to diminish the degree of conformational rotation due to the intramolecular hydrogen bonds leading to increased planarity and conjugation.<sup>36,37</sup> If a similar intramolecular locking could be introduced into the distorted lactam units, the desired motif would be harvested. Herein, an isomer of DPP was designed with two six-membered rings connected, named 4,4'-dialkyl-[6,6'-bithieno[3,2-*b*]pyridine]-5,5'-(4*H*,4'*H*)-dione (BTP) (Scheme 1). This new lactam motif is supposed to lock itself by intramolecular hydrogen bonds but with a distorted angle due to the steric hindrance of the increased ring size.

Besides, in ordinary organic solvents, the solubility of the conjugated polymers based on lactam skeletons can be well

<sup>a</sup> College of Polymer Science & Engineering, State Key Laboratory of Polymer Materials Engineering, Sichuan University, Chengdu 610065, China.  
E-mail: yxxu@scu.edu.cn

<sup>b</sup> State Key Laboratory of Luminescent Materials and Devices, School of Materials Science and Engineering, South China University of Technology, Guangzhou 510640, China

† Electronic supplementary information (ESI) available: Details of the experimental section, device fabrication and characterization, carrier mobility measurements, and other figures and tables. CCDC 1941412. For ESI and crystallographic data in CIF or other electronic format see DOI: 10.1039/c9tc04014e

regulated by incorporating alkyl side chains at the N-atom position.<sup>38,39</sup> Further selection of the optimum side chains could slightly adjust the frontier molecular orbital energy levels of the organic semiconductors, regulate the intermolecular packing and optimize the blend film morphology.<sup>38,40–42</sup> Consequently, great efforts have been devoted to developing a high-performance conjugated polymer by side-chain engineering.<sup>40,43–45</sup> Specifically, the length of the alkyl side chains plays a critical role in boosting the optoelectronic properties of the organic semiconductors.<sup>40,43,46</sup> It would be critical to attach specific alkyl side chains on newly designed lactam units to provide the solubility and form appropriate morphology resulting in optimum device performance in PSCs.

In this work, a novel distorted lactam unit BTP was designed and synthesized with intramolecular hydrogen bonds proved by single-crystal analysis. In addition, BTP allowed for introducing alkyl side chains of different lengths at the N-atom position. Based on the above advantages of BTP, two D–A conjugated polymers PBBDT-BTP-HD and PBBDT-BTP-OD with two different long side chains using 4,8-bis(5-(2-ethylhexyl)thiophen-2-yl)benzo[1,2-*b*:4,5-*b'*]dithiophene (BDT) as the donor unit and BTP as the acceptor unit were prepared. Furthermore, the photophysical, electrochemical and photovoltaic properties of both polymers were investigated to reveal the potential of BTP as a building block in PSCs.

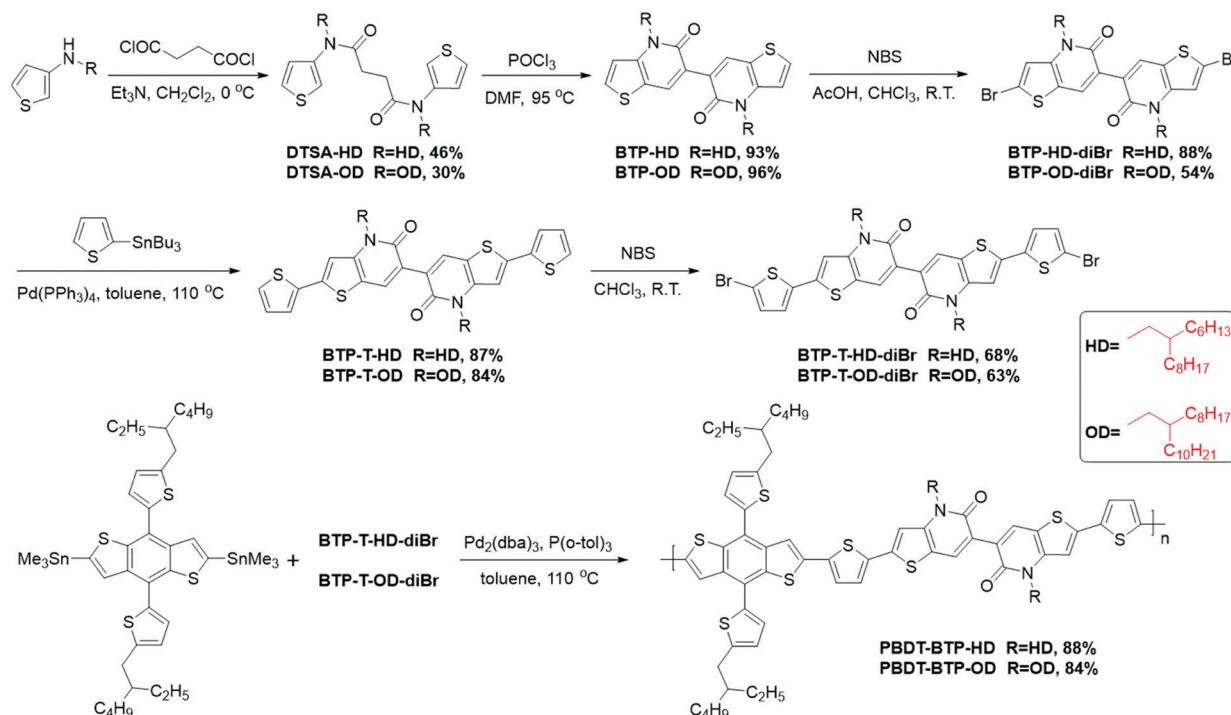
## Results and discussion

The detailed synthetic route of monomers and polymers is shown in Scheme 2. The intermediate amides were obtained

by condensation reaction between succinyl dichloride and *N*-alkylthiophen-3-amine. Subsequently, the intermediate amides were cyclized using the Vilsmeier reagent to afford the desired products BTP in good yields. The synthesis of key comonomers BTP-T-HD-diBr and BTP-T-OD-diBr consisted of three steps, including bromination of intermediate BTPs, coupling with 2-tributylstannyl-thiophene and bromination of the products again. Finally, the alternating polymers PBBDT-BTP-HD and PBBDT-BTP-OD were gained by copolymerizing lactam monomers with 2,6-bis(trimethyltin)-4,8-bis(5-(2-ethylhexyl)thiophen-2-yl)benzo[1,2-*b*:4,5-*b'*]dithiophene (BDT-diTin) using Pd<sub>2</sub>(dba)<sub>3</sub> and P(*o*-tol)<sub>3</sub> as catalysts. The resulting polymers had good solubility in chlorinated solvents, such as chloroform (CHCl<sub>3</sub>), chlorobenzene (CB) and dichlorobenzene (DCB). The number-average molecular weight (*M*<sub>n</sub>) of PBBDT-BTP-HD and PBBDT-BTP-OD was 7.05 and 7.85 kDa with a polydispersity index (PDI) of 3.33 and 2.93, respectively, evaluated by high-temperature gel permeation chromatography at 150 °C by using 1,2,4-trichlorobenzene as the eluent and linear polystyrene as the reference.

Thermogravimetric analysis (TGA) and differential scanning calorimetry (DSC) were used to investigate the thermal properties of PBBDT-BTP-HD and PBBDT-BTP-OD. The resulting curves are shown in Fig. S1, ESI.† Both the polymers presented good thermal stability and the thermal decomposition temperatures (*T*<sub>d</sub>, 5% weight loss) were over 390 °C, which was sufficient for application in polymer solar cells. There were no obvious thermal transitions during heating up to 250 °C, which implied that PBBDT-BTP-HD and PBBDT-BTP-OD possessed amorphous nature.

The analysis of single crystal X-ray diffraction (XRD) was performed to obtain insight into the conformation of lactam



Scheme 2 The synthetic route of PBBDT-BTP-HD and PBBDT-BTP-OD.

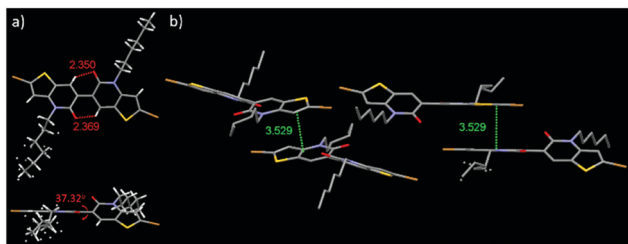


Fig. 1 (a) Single crystal structure and (b) molecular stacking structure of BTP-diBr. C (grey), H (white), O (red), N (blue), S (yellow), Br (brown). H···O and  $\pi$ - $\pi$  distance are marked and the unit is Å. Free solvent is hidden to provide an unobstructed view of BTP-diBr.

unit BTP. Single crystals of the hexyl-substituted BTP-diBr were gained by the slow diffusion of methanol into the chloroform solution. The molecular stacking of BTP-diBr is shown in Fig. 1, and the crystallographic data are listed in Table S2 (CCDC 1941412) (ESI†). The monoclinic crystal structure with space group  $P2_1/c$  was displayed in the single crystal of BTP-diBr. The backbone of BTP-diBr shows non-planar conformation with the torsional angle ( $37.31^\circ$ ) in favour of weakening intermolecular aggregation. There are two types of intramolecular hydrogen bonds (H···O) observed and the H···O bond distances are 2.350 and 2.369 Å, respectively. Therefore, BTP-diBr possessed a rigid and distorted conformation. In contrast, DPP-diBr displays a quasi-planar structure with the torsional angle of  $6.97^\circ$  (CCDC 1020305, see Fig. S2 in ESI†).<sup>47</sup> Furthermore, intermolecular  $\pi$ - $\pi$  stacking occurs for the half-unit of BTP-diBr owing to the non-planar structure. And the  $\pi$ - $\pi$  stacking distance is 3.529 Å

which is far greater than that in the DPP-diBr single crystal (3.320 Å), indicating that the  $\pi$ - $\pi$  interaction is weaker in BTP-diBr than in DPP-diBr.

The UV-vis absorption spectra of PBDT-BTP-HD and PBDT-BTP-OD in CB solution at different temperatures are depicted in Fig. 2a and b. As the temperature of the polymer solution increased from 25 to 95 °C, the absorption strength of the shoulder peak gradually weakened. The phenomenon could be ascribed to the dissociation of intermolecular aggregation or the weakening of the polymer backbone coplanarity. To clarify this phenomenon, the dependence of absorbance with concentration was measured for PBDT-BTP-HD and PBDT-BTP-OD at 583 nm. The results showed a linear relationship between absorbance and concentration (Fig. S3a, ESI†), indicating that no intermolecular aggregation occurred in the diluted CB solution. Therefore, it is speculated that both the polymers possessed strong intramolecular hydrogen bonds in CB solution at low temperatures. With the elevation of the temperature, the intramolecular hydrogen bonds were gradually weakened and the coplanarity of the backbone was reduced. Therefore, the shoulder peak was diminished. Compared with the polymer solution, the films showed slightly red-shifted absorption peaks (Fig. 2c), demonstrating that further intermolecular aggregation occurred. Notably, the annealed films of both the polymers showed lowered shoulder peaks (Fig. S3b, ESI†) compared to the unannealed one, which was probably originated from the weakening of intramolecular hydrogen bonding. According to the calculation results (Fig. 3), the dihedral angles among the units are below  $25^\circ$ , much lower than the values observed in the single crystal. It is possible that the packing of polymer chains

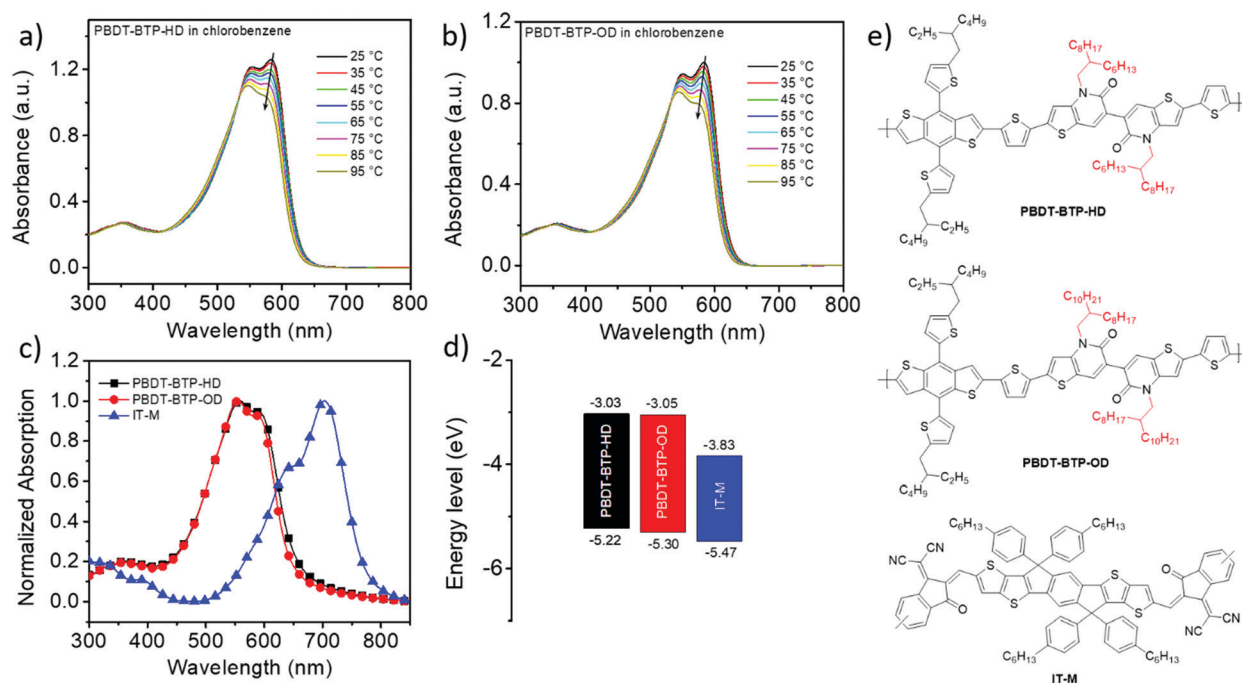


Fig. 2 (a and b) Temperature dependent UV-vis absorption spectra of PBDT-BTP-HD and PBDT-BTP-OD in chlorobenzene solution; (c) UV-vis film absorption spectra, (d) energy level diagram and (e) chemical structure of PBDT-BTP-HD, PBDT-BTP-OD and IT-M.

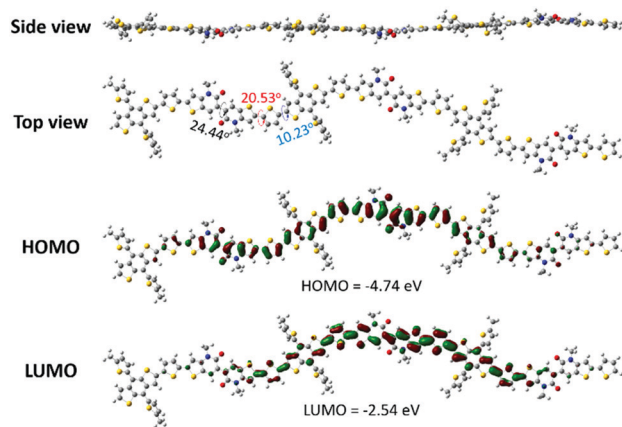


Fig. 3 Optimized molecular conformations and energy levels of polymer calculated by DFT at the B3LYP/6-31G\* level.

will force the lactam unit to rotate into a larger dihedral angle, thus resulting in lower conjugation in the solid state. It is also encouraging that both the polymers possessed complementary absorption with the electron acceptor, IT-M (Fig. 2c and Fig. S4a, ESI<sup>†</sup>), which is beneficial for the light absorption of devices. The key optical parameters are summarized in Table 1.

The molecular energy levels were measured by using the cyclic voltammetry (CV) method. The CV curves of PBDT-BTP-HD and PBDT-BTP-OD are shown in Fig. S4b, ESI<sup>†</sup>. The corresponding highest occupied molecular orbital (HOMO) and the lowest unoccupied molecular orbital (LUMO) energy levels of PBDT-BTP-HD and PBDT-BTP-OD were  $-5.22/-3.03$  and  $-5.30/-3.05$  eV, respectively. The LUMO levels remain similar but the HOMO levels tend to decrease as the length of the side chains increases. This suggests that the steric hindrance of the longer side chains led to looser packing and reduced electronic coupling between the polymer backbones. The HOMO/LUMO levels of both polymers matched well with IT-M for PSCs. The electrochemical band gaps of PBDT-BTP-HD and PBDT-BTP-OD were estimated to be 2.19 and 2.25 eV (Table 1) respectively, which was consistent with their optical bandgaps. Density functional theory (DFT) calculation at the B3LYP/6-31G\* level was performed to obtain optimized geometries and energy levels of three repetitive units of polymer. As shown in Fig. 3, both HOMO and LUMO orbitals were reasonably delocalized along the polymer backbone in the optimal geometries. The calculated HOMO and LUMO energy levels of the polymer are  $-4.74$  and  $-2.54$  eV, which agrees with the trend of the cyclic voltammetry test.

The X-ray diffraction (XRD) analysis was carried out to study the stacking in PBDT-BTP-HD and PBDT-BTP-OD films before and after annealing. As shown in Fig. S5 (ESI<sup>†</sup>), PBDT-BTP-HD

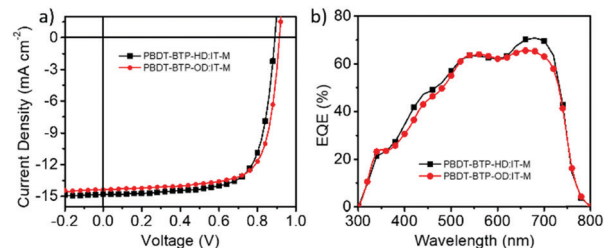


Fig. 4 (a) The  $J-V$  curves of the PSCs based on PBDT-BTP-HD:IT-M and PBDT-BTP-OD:IT-M and (b) the EQE spectra of the corresponding PSCs.

and PBDT-BTP-OD films displayed the diffraction peaks at  $2\theta = 24.40^\circ$  and  $24.28^\circ$  before annealing corresponding to  $\pi-\pi$  stacking distance of 3.645 and 3.663 Å, respectively. The results implied that PBDT-BTP-HD with a short side chain had more compact stacking, which might lead to a higher hole mobility. After annealing, the PBDT-BTP-HD and PBDT-BTP-OD films presented a smaller  $\pi-\pi$  stacking distance of 3.639 and 3.660 Å ( $2\theta = 24.44^\circ$  and  $24.30^\circ$ ), which implied that annealing was conducive to polymer stacking.

To evaluate the photovoltaic properties of PBDT-BTP-HD and PBDT-BTP-OD as donor materials in BHJ polymer solar cells, the devices were fabricated with the inverted configuration indium tin oxide (ITO)/ZnO/donor polymer:IT-M/MoO<sub>3</sub>/Ag. The current density-voltage ( $J-V$ ) curves of the PSCs were measured under simulated AM 1.5G illumination at  $100 \text{ mW cm}^{-2}$  and shown in Fig. 4a and associated data of the PSCs are presented in Table 2. The optimized conditions of device fabrication are summarized in Tables S3–S5 (ESI<sup>†</sup>). The maximum PCE for PBDT-BTP-HD and PBDT-BTP-OD devices was obtained by adding 1% (v/v) 1,8-diiodooctane (DIO) as additive followed by a thermal annealing at  $120^\circ\text{C}$  and  $140^\circ\text{C}$  for 10 min, respectively. The PSC based on PBDT-BTP-HD:IT-M (1:1, w/w) showed an impressive PCE of 9.47%, with an open-circuit voltage ( $V_{oc}$ ) of 0.89 V, a short-circuit current density ( $J_{sc}$ ) of  $14.82 \text{ mA cm}^{-2}$ , and a fill factor (FF) of 71.78%. Besides, the device based on PBDT-BTP-OD:IT-M (1:1.5, w/w) generated a comparable PCE of 9.54%, with slightly enhanced  $V_{oc}$  of 0.91 V and FF of 72.66%, and decreased  $J_{sc}$  of  $14.38 \text{ mA cm}^{-2}$ . The improved  $V_{oc}$  value originated from the lower-lying HOMO energy level of PBDT-BTP-OD and the diminished  $J_{sc}$  might be attributed to weaker absorbance of PBDT-BTP-OD. The PSC devices based on PBDT-BTP-HD:IT-M and PBDT-BTP-OD:IT-M exhibited a broad response from 300 to 800 nm because of good complementary absorption. The external quantum efficiency (EQE) measurements were used to verify the  $J_{sc}$  values and are shown in Fig. 4b and Fig. S6, ESI<sup>†</sup>. The calculated  $J_{sc}$  values ( $J_{cal}$ ) by integration of

Table 1 Optical and electrochemical properties of PBDT-BTP-HD and PBDT-BTP-OD

Polymer	$\lambda_{\text{max,solution}}$ (nm)	$\epsilon_{\text{solution}}$ ( $\text{M}^{-1} \text{ cm}^{-1}$ )	$\lambda_{\text{max,film}}$ (nm)	$\lambda_{\text{edge}}$ (nm)	$E_g^{\text{opt}}$ (eV)	$E_{\text{HOMO}}$ (eV)	$E_{\text{LUMO}}$ (eV)	$E_g^{\text{CV}}$ (eV)
PBDT-BTP-HD	554, 583	$5.4 \times 10^4$	558, 586	652	1.90	$-5.22$	$-3.03$	2.19
PBDT-BTP-OD	551, 584	$4.5 \times 10^4$	555, 587	645	1.92	$-5.30$	$-3.05$	2.25

Table 2 Device parameters of the PSCs based on PBDT-BTP-HD:IT-M and PBDT-BTP-OD:IT-M

Active layer	$V_{oc}$ (V)	$J_{sc}$ (mA cm <sup>-2</sup> )	$J_{cal}^a$ (mA cm <sup>-2</sup> )	FF (%)	PCE <sub>max</sub> (PCE <sub>ave</sub> ) <sup>b</sup> (%)
PBDT-BTP-HD:IT-M	0.89	14.82	14.09	71.78	9.47 (9.18 ± 0.20)
PBDT-BTP-OD:IT-M	0.91	14.38	13.56	72.66	9.54 (9.25 ± 0.17)

<sup>a</sup> The  $J_{cal}$  values were determined from the integration of the related EQE curves. <sup>b</sup> The average PCE was obtained from at least 10 devices.

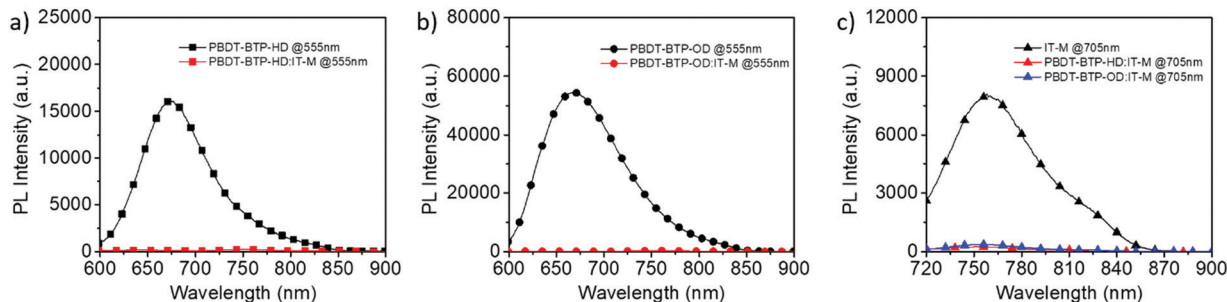


Fig. 5 Photoluminescence spectra for (a) PBDT-BTP-HD and blend films excited at 555 nm; (b) PBDT-BTP-OD and blend films excited at 555 nm; (c) IT-M and blend films excited at 705 nm.

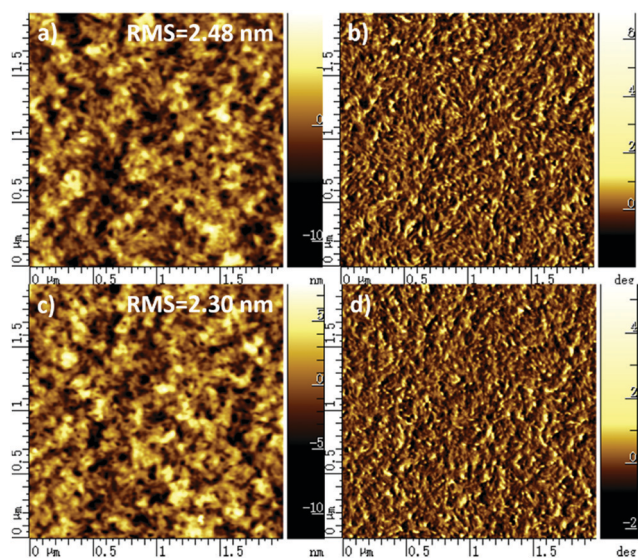


Fig. 6 AFM height (left) and phase (right) images of (a and b) PBDT-BTP-HD:IT-M and (c and d) PBDT-BTP-OD:IT-M blend films with DIO as additive.

the EQE curves were in good agreement with those obtained from the  $J$ - $V$  measurements.

The exciton dissociation and charge transfer in the active layers were estimated by photoluminescence (PL) quenching experiments. As illustrated in Fig. 5, the emissions for PBDT-BTP-HD:IT-M and PBDT-BTP-OD:IT-M were highly quenched when excited at 555 nm, revealing an effective electron transfer from polymers to acceptors. The emission quenching for the PBDT-BTP-HD:IT-M film was more notable than that of the PBDT-BTP-OD:IT-M film when excited at 705 nm. The results suggested that devices based on PBDT-BTP-HD:IT-M could form more efficient charge separation, which agreed well with higher  $J_{sc}$  in the related PSCs.

The hole and electron mobility ( $\mu_h$  and  $\mu_e$ ) of the active layers were measured through the space charge limited current (SCLC) method, and the related charts are depicted in Fig. S7 and Table S6, ESI†. The blend films of PBDT-BTP-HD:IT-M exhibited higher hole mobility ( $7.67 \times 10^{-4}$  cm<sup>2</sup> V<sup>-1</sup> s<sup>-1</sup>) than those of the PBDT-BTP-OD:IT-M films ( $7.30 \times 10^{-4}$  cm<sup>2</sup> V<sup>-1</sup> s<sup>-1</sup>), but the former presented lower electron mobility ( $1.12 \times 10^{-4}$  cm<sup>2</sup> V<sup>-1</sup> s<sup>-1</sup>) than the latter ( $5.42 \times 10^{-4}$  cm<sup>2</sup> V<sup>-1</sup> s<sup>-1</sup>). As a result, the  $\mu_h/\mu_e$  ratio based on the PBDT-BTP-OD:IT-M film (1.35) was more balanced than that of the PBDT-BTP-HD:IT-M film (6.85), which could be responsible for the higher FF (72.66%) of related devices.

The morphologies of the active layers were investigated by using an atomic force microscope (AFM). As shown in Fig. 6, the PBDT-BTP-OD:IT-M film appeared with a slightly smoother surface with the root mean square (RMS) roughness of 2.30 nm compared with the PBDT-BTP-HD:IT-M film (RMS = 2.48 nm). The higher roughness could be derived from a more compact stacking of the PBDT-BTP-HD film as proved in the XRD pattern. The molecular orientation and packing of the pristine and blend films were investigated through grazing incidence wide-angle X-ray scattering (GIWAXS) measurements. The GIWAXS patterns and their corresponding line-cut profiles are shown in Fig. 7 and Fig. S8 (ESI†), respectively. PBDT-BTP-HD and PBDT-BTP-OD pristine films showed an obvious  $\pi$ - $\pi$  stacking peak (010) at 1.68 and 1.66 Å<sup>-1</sup> (3.74 and 3.79 Å) along the out-of-plane direction, which indicated that the neat polymer films took face-on orientation. IT-M was also inclined to adopt face-on orientation. While in the blend films, PBDT-BTP-OD:IT-M still maintained face-on orientation which was in favour of vertical charge transport, resulting in a more balanced carrier mobility and a higher FF. In comparison, the PBDT-BTP-HD:IT-M blend film showed mixed face-on and edge-on orientation, which explains the inferior balance of hole and electron transport and lower FF value.

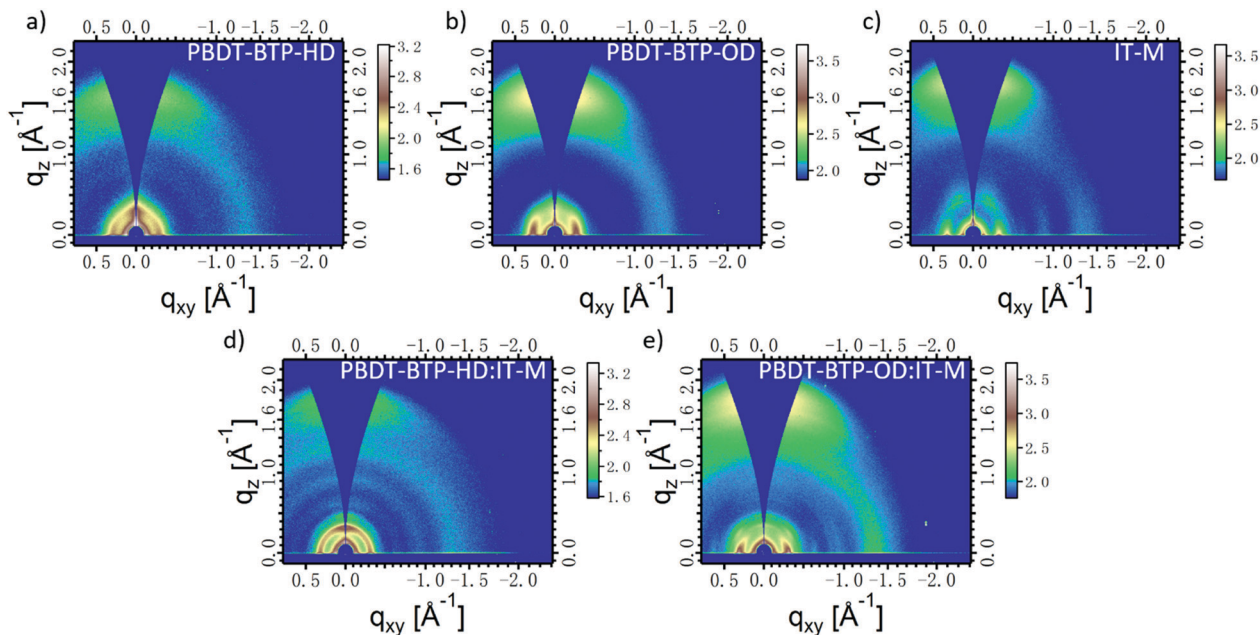


Fig. 7 The GIWAXS patterns of (a) PBDT-BTP-HD; (b) PBDT-BTP-OD; (c) IT-M; (d) PBDT-BTP-HD:IT-M and (e) PBDT-BTP-OD:IT-M.

## Conclusions

A novel distorted lactam skeleton BTP with intramolecular H···O interactions was synthesized and characterized. Two conjugated polymers PBDT-BTP-HD and PBDT-BTP-OD, composed of BDT as a donor unit and BTP as an acceptor unit, were developed with two different long side chains. PBDT-BTP-OD exhibited a deeper HOMO level and more balanced carrier mobility than PBDT-BTP-HD, but the latter exhibited a higher absorption coefficient and more compact stacking than the former. Taking the above factors, both the polymers demonstrated comparable PCEs. As a result, the non-fullerene PSCs based on PBDT-BTP-OD with IT-M showed power conversion efficiency of up to 9.54% benefitting from side-chain engineering. Thus, it is strongly believed that the novel distorted lactam BTP is a promising skeleton in organic solar cells.

## Conflicts of interest

There are no conflicts to declare.

## Acknowledgements

Y.-X. X. acknowledges the financial support from the National Natural Science Foundation of China (51403135) and Sichuan Science and Technology Program (Grant No. 2019YJ0123).

## Notes and references

- G. Yu, J. Gao, J. C. Hummelen, F. Wudl and A. J. Heeger, *Science*, 1995, **270**, 1789.
- Z. Xiao, X. Jia and L. Ding, *Sci. Bull.*, 2017, **62**, 1562–1564.

- L. Meng, Y. Zhang, X. Wan, C. Li, X. Zhang, Y. Wang, X. Ke, Z. Xiao, L. Ding, R. Xia, H.-L. Yip, Y. Cao and Y. Chen, *Science*, 2018, **361**, 1094–1098.
- P. Cheng, G. Li, X. Zhan and Y. Yang, *Nat. Photonics*, 2018, **12**, 131–142.
- J. Hou, O. Inganäs, R. H. Friend and F. Gao, *Nat. Mater.*, 2018, **17**, 119.
- C. Yan, S. Barlow, Z. Wang, H. Yan, A. K. Y. Jen, S. R. Marder and X. Zhan, *Nat. Rev. Mater.*, 2018, **3**, 18003.
- K. Feng, J. Yuan, Z. Bi, W. Ma, X. Xu, G. Zhang and Q. Peng, *iScience*, 2019, **12**, 1–12.
- G. Zhang, J. Zhao, P. C. Y. Chow, K. Jiang, J. Zhang, Z. Zhu, J. Zhang, F. Huang and H. Yan, *Chem. Rev.*, 2018, **118**, 3447–3507.
- B. Kan, H. Feng, H. Yao, M. Chang, X. Wan, C. Li, J. Hou and Y. Chen, *Sci. China: Chem.*, 2018, **61**, 1307–1313.
- H. Zhang, H. Yao, J. Hou, J. Zhu, J. Zhang, W. Li, R. Yu, B. Gao, S. Zhang and J. Hou, *Adv. Mater.*, 2018, **30**, 1800613.
- H. Yao, Y. Cui, D. Qian, C. S. Ponseca, Jr., A. Honarfar, Y. Xu, J. Xin, Z. Chen, L. Hong, B. Gao, R. Yu, Y. Zu, W. Ma, P. Chabera, T. Pullerits, A. Yartsev, F. Gao and J. Hou, *J. Am. Chem. Soc.*, 2019, **141**, 7743–7750.
- J. Yuan, Y. Zhang, L. Zhou, C. Zhang, T. K. Lau, G. Zhang, X. Lu, H. L. Yip, S. K. So, S. Beaupre, M. Mainville, P. A. Johnson, M. Leclerc, H. Chen, H. Peng, Y. Li and Y. Zou, *Adv. Mater.*, 2019, **31**, 1807577.
- B. B. Fan, D. F. Zhang, M. J. Li, W. K. Zhong, Z. M. Y. Zeng, L. Ying, F. Huang and Y. Cao, *Sci. China: Chem.*, 2019, **62**, 746–752.
- Y. Cui, H. Yao, L. Hong, T. Zhang, Y. Xu, K. Xian, B. Gao, J. Qin, J. Zhang, Z. Wei and J. Hou, *Adv. Mater.*, 2019, **31**, 1808356.
- J. Yuan, Y. Zhang, L. Zhou, G. Zhang, H.-L. Yip, T.-K. Lau, X. Lu, C. Zhu, H. Peng, P. A. Johnson, M. Leclerc, Y. Cao, J. Ulanski, Y. Li and Y. Zou, *Joule*, 2019, **3**, 1140–1151.

- 16 Y. Cui, H. Yao, J. Zhang, T. Zhang, Y. Wang, L. Hong, K. Xian, B. Xu, S. Zhang, J. Peng, Z. Wei, F. Gao and J. Hou, *Nat. Commun.*, 2019, **10**, 2515.
- 17 X. Xu, K. Feng, Z. Bi, W. Ma, G. Zhang and Q. Peng, *Adv. Mater.*, 2019, **31**, 1901872.
- 18 D. Liu, B. Yang, B. Jang, B. Xu, S. Zhang, C. He, H. Y. Woo and J. Hou, *Energy Environ. Sci.*, 2017, **10**, 546–551.
- 19 S. Li, L. Ye, W. Zhao, H. Yan, B. Yang, D. Liu, W. Li, H. Ade and J. Hou, *J. Am. Chem. Soc.*, 2018, **140**, 7159–7167.
- 20 S. Zhang, Y. Qin, J. Zhu and J. Hou, *Adv. Mater.*, 2018, **30**, 1800868.
- 21 Y. Deng, J. Liu, J. Wang, L. Liu, W. Li, H. Tian, X. Zhang, Z. Xie, Y. Geng and F. Wang, *Adv. Mater.*, 2014, **26**, 471–476.
- 22 W. Yue, R. S. Ashraf, C. B. Nielsen, E. Collado-Fregoso, M. R. Niazi, S. A. Yousaf, M. Kirkus, H. Y. Chen, A. Amassian, J. R. Durrant and I. McCulloch, *Adv. Mater.*, 2015, **27**, 4702–4707.
- 23 X. Song, N. Gasparini, M. M. Nahid, S. H. K. Paleti, C. Li, W. Li, H. Ade and D. Baran, *Adv. Funct. Mater.*, 2019, **29**, 1902441.
- 24 M. An, F. Xie, X. Geng, J. Zhang, J. Jiang, Z. Lei, D. He, Z. Xiao and L. Ding, *Adv. Energy Mater.*, 2017, **7**, 1602509.
- 25 D. Li, Z. Xiao, S. Z. Wang, X. J. Geng, S. F. Yang, J. F. Fang, H. Yang and L. M. Ding, *Adv. Energy Mater.*, 2018, **8**, 1800397.
- 26 A. M. Schneider, L. Lu, E. F. Manley, T. Zheng, V. Sharapov, T. Xu, T. J. Marks, L. X. Chen and L. Yu, *Chem. Sci.*, 2015, **6**, 4860–4866.
- 27 W. Li, K. H. Hendriks, M. M. Wienk and R. A. Janssen, *Acc. Chem. Res.*, 2016, **49**, 78–85.
- 28 H.-C. Wang, J. Tao, W.-Y. Bai, Z.-Y. Xie, H. Li, X. Ren and Y.-X. Xu, *Eur. J. Org. Chem.*, 2018, 1218–1223.
- 29 P. E. Hartnett, A. Timalisina, H. S. Matte, N. Zhou, X. Guo, W. Zhao, A. Facchetti, R. P. Chang, M. C. Hersam, M. R. Wasielewski and T. J. Marks, *J. Am. Chem. Soc.*, 2014, **136**, 16345–16356.
- 30 W. Wu, G. Zhang, X. Xu, S. Wang, Y. Li and Q. Peng, *Adv. Funct. Mater.*, 2018, **28**, 1707493.
- 31 Y. Duan, X. Xu, H. Yan, W. Wu, Z. Li and Q. Peng, *Adv. Mater.*, 2017, **29**, 1605115.
- 32 Y. Qin, S. Liu, H. Gu, W. Dai and X. Luo, *Sol. Energy*, 2018, **166**, 450–457.
- 33 S. Ko, E. T. Hoke, L. Pandey, S. Hong, R. Mondal, C. Risko, Y. Yi, R. Noriega, M. D. McGehee, J. L. Bredas, A. Salleo and Z. Bao, *J. Am. Chem. Soc.*, 2012, **134**, 5222–5232.
- 34 H. Li, Y. J. Hwang, B. A. Courtright, F. N. Eberle, S. Subramaniyan and S. A. Jenekhe, *Adv. Mater.*, 2015, **27**, 3266–3272.
- 35 D. Meng, H. Fu, C. Xiao, X. Meng, T. Winands, W. Ma, W. Wei, B. Fan, L. Huo, N. L. Doltsinis, Y. Li, Y. Sun and Z. Wang, *J. Am. Chem. Soc.*, 2016, **138**, 10184–10190.
- 36 L. Dou, J. Gao, E. Richard, J. You, C. C. Chen, K. C. Cha, Y. He, G. Li and Y. Yang, *J. Am. Chem. Soc.*, 2012, **134**, 10071–10079.
- 37 L. Dou, W. H. Chang, J. Gao, C. C. Chen, J. You and Y. Yang, *Adv. Mater.*, 2013, **25**, 825–831.
- 38 W. Li, K. H. Hendriks, A. Furlan, W. S. Roelofs, S. C. Meskers, M. M. Wienk and R. A. Janssen, *Adv. Mater.*, 2014, **26**, 1565–1570.
- 39 W. S. Yoon, D. W. Kim, J.-M. Park, I. Cho, O. K. Kwon, D. R. Whang, J. H. Kim, J.-H. Park and S. Y. Park, *Macromolecules*, 2016, **49**, 8489–8497.
- 40 J. Shin, G. E. Park, D. H. Lee, H. A. Um, T. W. Lee, M. J. Cho and D. H. Choi, *ACS Appl. Mater. Interfaces*, 2015, **7**, 3280–3288.
- 41 Z.-G. Zhang and Y. Li, *Sci. China: Chem.*, 2014, **58**, 192–209.
- 42 L. Yang, H. Zhou and W. You, *J. Phys. Chem. C*, 2010, **114**, 16793–16800.
- 43 I. Meager, R. S. Ashraf, S. Mollinger, B. C. Schroeder, H. Bronstein, D. Beatrup, M. S. Vezie, T. Kirchartz, A. Salleo, J. Nelson and I. McCulloch, *J. Am. Chem. Soc.*, 2013, **135**, 11537–11540.
- 44 L. Lu, T. Zheng, Q. Wu, A. M. Schneider, D. Zhao and L. Yu, *Chem. Rev.*, 2015, **115**, 12666–12731.
- 45 S. Nishinaga, H. Mori and Y. Nishihara, *Macromolecules*, 2015, **48**, 2875–2885.
- 46 X. Sun, Z. Zhang, R. Hou, M. Huang, B. Zhao and S. Tan, *Dyes Pigm.*, 2017, **139**, 403–411.
- 47 J. Roth-Barton and J. M. White, CCDC 1020305: Experimental Crystal Structure Determination, 2014, DOI: 10.5517/cc137q24.